

Phase Behavior of a Structurally Constrained Organic–Inorganic Crystal: Temperature-Dependent Infrared Spectroscopy of Silver *n*-Dodecanethiolate

Jean-François Bardeau,[†] Atul N. Parikh,* Jaime D. Beers,[‡] and Basil I. Swanson

Bioscience Division, Los Alamos National Laboratory, Los Alamos, New Mexico 87545

Received: June 25, 1999; In Final Form: October 6, 1999

Using temperature-dependent Fourier transform infrared (FTIR) spectroscopy, we probe the molecular level, chain-structural dynamics associated with solid–solid transitions between 25 and 250 °C in a layered inorganic–organic silver dodecanethiolate, $\text{AgS}(\text{CH}_2)_{11}\text{CH}_3$. Spectroscopic evidence presented here establishes two major transitions: the transition occurring at ~ 130 °C is characterized by an abrupt, but fully reversible, change in the chain conformational order from an initial all-trans state to the one characterized by mixed or partial chain disorder. The observation of this phase transition is consistent with the previous predictions of a rapid and drastic change in the structural motif from an initial bilayer to the final micellar state. The second transition at about 190 °C, which is consistent with the previous assignment of micellar amorphous transition, is furthermore irreversible and represents thermal degradation of the material. Implications of these results for the general family of chain molecular assemblies in constrained molecular environments are discussed.

Introduction

The classes of organic–inorganic heterostructures that exhibit alternating two-dimensional (2D) molecular assemblies of organic and inorganic constituents have expanded considerably now encompassing a host of technologically relevant materials including surfactant mesophases,¹ organic perovskites,² intercalated compounds,³ Langmuir–Blodgett films,⁴ liquid crystals,⁵ model biological lipid membranes,⁶ and self-assembled monolayers.^{7,8} Interest in developing key interrelationships that exist between their structure, molecular level dynamics, and macroscopic properties persists because of the vast array of possibilities they offer in manipulating specific material properties (e.g., stiffness, strength,⁹ weight, nonlinear optical behavior,¹⁰ electrical conductivity, photochemical charge transfer,¹¹ and ferromagnetism¹²) by systematic variations in the structure and properties of the organic and inorganic constituents at the molecular level.

Of particular interest to us is the correlation between molecular motions and the phase behavior or melting of 2D organic molecular (e.g., alkyl chain) assemblies. Previous efforts to this end have almost exclusively focused on the melting of aliphatic chain crystals,^{13,14} e.g., simple and substituted crystalline *n*-alkanes and long-chain phospholipids. In these materials, the chain motions imparted by the thermal energy are generally shown to be associated with the translational (lateral and transverse jumps of individual molecules from their parent ensembles), and rotational and torsional or conformational (trans–gauche isomerization) dynamics of the chains. But it is quite evident, e.g., in structurally complex organic–inorganic heterostructures above, that the strong coupling between the chain termini and the contiguous inorganic interface must influence the phase behavior and chain dynamics in nontrivial manner by constraining at least some of the above degrees of

freedom. In particular, such couplings may lead to frustrations in the out-of-plane mobilities of the chains in the 2D ensembles thereby effectively reducing the dimensionality or to frustrations in the in-plane lateral mobilities by restricting translational and thereby conformational disordering of the chains. Indeed, in the previous studies of substituted *n*-alkanes,¹⁵ liquid-crystalline mesophases,¹⁶ and biological lipids,¹⁷ the weak or nonbonded headgroup–headgroup interactions are believed to be responsible for the significant delays and broadening in the chain melting transition. In this regard, layered organic–inorganic hybrid materials provide limiting cases wherein the chain molecular assemblies are integrally tethered to their inorganic interfaces, for example, in nonmolecular covalent lamellar solids. Here, covalent coupling of the chains to a covalently coupled inorganic framework can effectively serve to preclude translational (lateral diffusion or longitudinal hopping) motions thereby disallowing melting of 2D chain assemblies by the loss of in-plane translational ordering. Furthermore, existing models of melting in 2D ensembles requires the decay of a translational order parameter.¹⁸ But when translational order parameter cannot significantly evolve, such as in the lamellar covalently tethered network solids,¹⁹ what motions and mobility determine the phase behavior and sequence of quasi-2D chain assemblies remains an intriguing issue. Clearly, a study aimed at delineating how the chain dynamics occur when thermal energy is imparted to covalent lamellar solids would offer new insights into the melting mechanism in restricted environments.

In this regard, the nonmolecular sheet compounds of long-chain silver (*n*-alkane) thiolates, $\text{AgS}(\text{CH}_2)_n\text{CH}_3$, first reported by Dance and co-workers,²⁰ provide an appropriately suited sample system. Here, we and others^{21–23} have shown that the trigonal coordination of Ag with S atoms forms a strongly coupled quasi-hexagonal 2D Ag–S lattice with alkyl chain substituents covalently linked to each S atom of the lattice and extending away on either side of the lattice in a perpendicular orientation. A schematic depiction of this structure of long chain substituted silver thiolates ($\text{AgS}(\text{CH}_2)_n\text{CH}_3$, $n = 6–18$) deduced previously using X-ray diffraction and vibrational spectroscopy

* Corresponding author. E-mail address: parikh@lanl.gov.

[†] Laboratoire de Physique de L'Etat Condense, Université du Maine, Le Mans, France.

[‡] Participant, Underrepresented and Minority Student Program, Los Alamos National Laboratory.

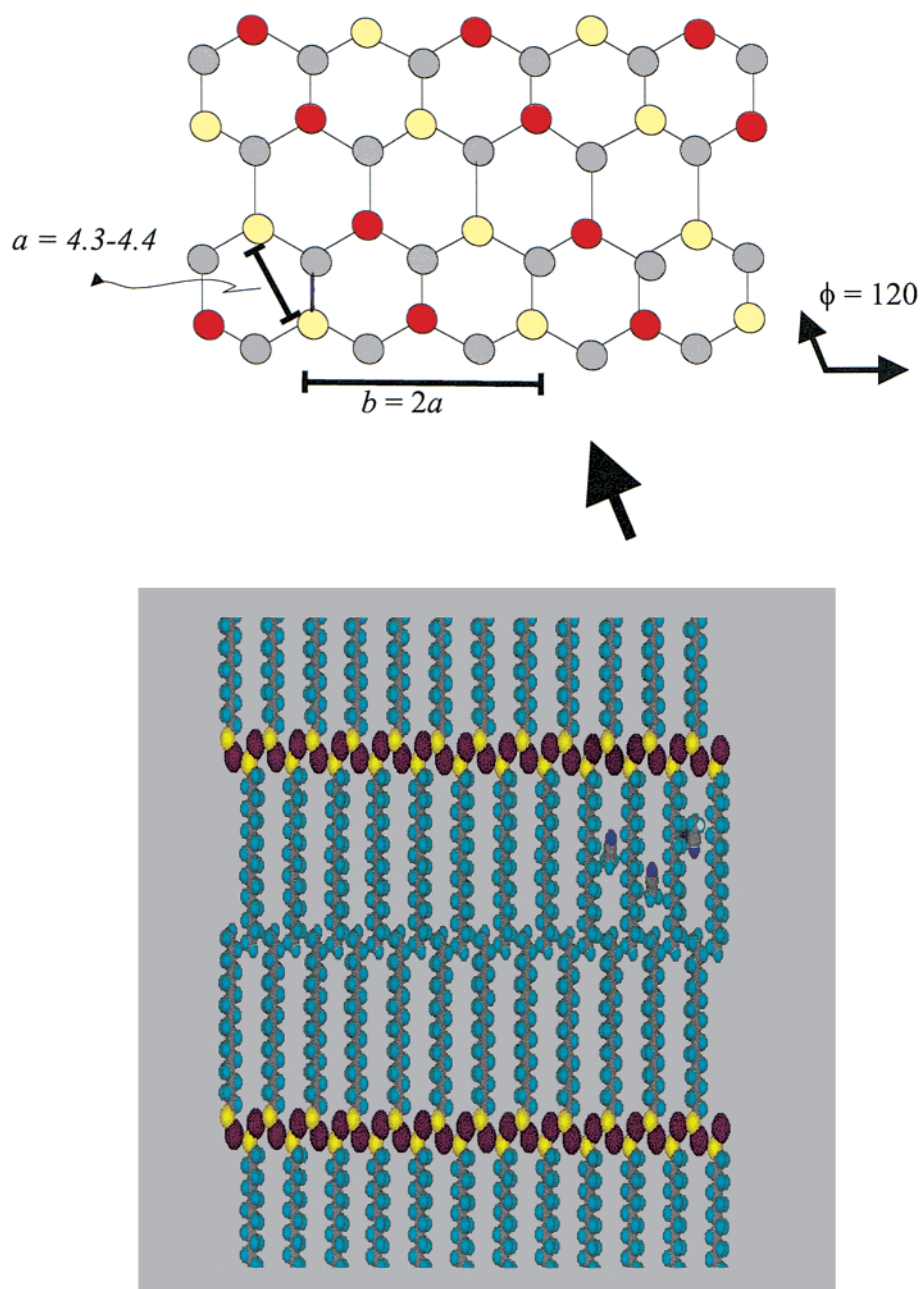


Figure 1. A schematic representation of the covalently bonded nonmolecular sheet structure of long chain silver *n*-alkanethiolates. Top panel approximates the pseudo-2D network of μ^3 bridged Ag (gray circles) and S atoms. Red circles represent the S atoms for whom the chain substituents extend out of the plane of paper while the yellow circles represent S with substituents projecting into the plane of the paper. Bottom panel approximates the perpendicular view along the direction of the arrow revealing all-trans extended chains and the Ag-S interface.

is shown in Figure 1. Although no molecular level studies (e.g., spectroscopic) that purportedly delineate the dynamics of chains have been reported, a recent study by Baena and co-workers,²¹ using DSC and powder XRD measurements, show that the long-chain silver (*n*-alkane) thiolates undergo a dominant melting, solid-solid phase transition associated with a dramatic structural change from an initial bilayer motif to a micellar motif, reminiscent of thermotropic behavior of liquid-crystalline mesogens.²⁴ Here, we present infrared vibrational spectroscopy evidence that reveals an abrupt change in the chain conformational and packing properties at this transition. Specifically, using temperature-dependent Fourier transform infrared spectra during repeated thermal cycles between 25 °C and the maximum of 250 °C, we show that the dominant solid-solid bilayer-micellar transition is attended by an abrupt, but fully reversible, rise in the gauche conformers between 125 and 135 °C with a

concomitant change in the packing of the aliphatic tails from an initial, efficient hexagonal type to the final one characterized by a highly disordered packing of partially aligned alkyl chains. These observations are fully consistent with the earlier predictions of the abrupt mesoscopic change in the structural motif from bilayer to micellar geometry at ~ 130 °C. Moreover, present data further reveal a weak but distinct "premelting" event wherein the gradual accumulation of gauche conformers in small but nonvanishing population between 100 and 125 °C prepares the material system for the bilayer-micellar transition. Our data further show that the micellar state is stable up to ~ 175 °C but irreversibly disorders between 175 and 200 °C into an amorphous or liquidlike state with highly disordered alkyl chains. The irreversibility of the latter transition in conjunction with the irreversible loss of spectral intensities due to alkyl chain

signals that this second transition at ~ 190 °C is associated with the thermal degradation of the material.

Experimental Details

$\text{CH}_3(\text{CH}_2)_{11}\text{SAg}$ or silver *n*-dodecanethiolate was prepared according to a previously published procedure.²³ Briefly, to an equimolar mixture of an *n*-dodecanethiol (4 mM) and triethylamine (4 mM) in acetonitrile was added silver nitrate solution (4 mM), also in acetonitrile, in a dropwise manner at a constant rate of addition (0.3–0.5 mL/min). The solution mixture was held under constant stirring at room temperature during the reaction period (~ 12 – 15 h). Exposure to laboratory light was minimized by wrapping all reaction vessels with several layers of aluminum foil. The precipitate was collected by suction filtration, thoroughly washed with acetonitrile, and then dried under vacuum at room temperature. The collected solid was stored in a dry atmosphere until further use.

Temperature-dependent infrared spectra were collected using a Bruker IFS55 Fourier transform infrared spectrophotometer equipped with a DTGS detector (Bruker, Gottingen, Germany). The sample chamber was a commercial variable temperature cell (Graseby Speacac, Smyrna, GA) equipped with an evacuable jacket, a refrigerant chamber, and a stainless steel sample holder. Sample temperature was monitored using a copper–constantan thermocouple placed in very close vicinity of the sample. The temperature control to within 0.5 deg was achieved using an automatic temperature controller (Graseby Speacac, Smyrna, GA) over the temperature range 25–250 °C. The sample cell was evacuated to below 0.01 Torr during all measurements. The sample consisted of pellets prepared by pressing a mechanically homogenized mixture of the dried silver dodecanethiolate with nominally dehydrated pure KBr. The spectra were obtained at nominally 2 cm^{-1} resolution. For more precise determination of peak positions, the interferograms were zero-filled to increase the point density by a factor of 2. All spectra are reported in the transmission absorbance units, $A = -\log(T/T_0)$, where T and T_0 are the power spectra of each sample and reference, respectively. The data analysis was performed using Grams 32 (SpectraCalc) software for peak-fitting and analyses.

Results

Room temperature transmission infrared spectrum for $\text{AgS}(\text{CH}_2)_{11}\text{CH}_3$ is shown in Figure 2. All observed peaks in the mid-infrared region can be straightforwardly and accurately assigned to specific chain vibrational modes by simply following previous reports of the vibrational mode assignments for simple and substituted *n*-alkanes of comparable chain-lengths.^{15,25–28}

The higher frequency region, 2800 – 3000 cm^{-1} , in Figure 2a reveals the presence of four distinct peaks, assigned to methylene and methyl stretching modes. In particular, the bands near 2848 and 2916 cm^{-1} are assigned to the symmetric ($\nu_s(\text{CH}_2)$, d^+) and asymmetric stretching vibrations ($\nu_{as}(\text{CH}_2)$, d^-) of the methylene groups, respectively. The two weaker but distinct peaks observed at ~ 2873 and 2953 cm^{-1} are assigned to the symmetric ($\nu_s(\text{CH}_3)$, r^+) and asymmetric stretching vibrations ($\nu_{as}(\text{CH}_3)$, r^-) of the methyl group. Additionally, overlapping weaker and broader peaks at ~ 2895 and 2935 cm^{-1} are also observed and can be attributed to Fermi resonances absorption due to d^+ and r^+ modes, respectively.²⁵ It is well appreciated in the past literature that the d^+ and d^- bands are strong indicators of the chain conformation: the peak frequencies of the CH_2 stretching modes of alkyl chains are typically reported to lie in the narrow ranges of 2846 – 2850 and 2915 –

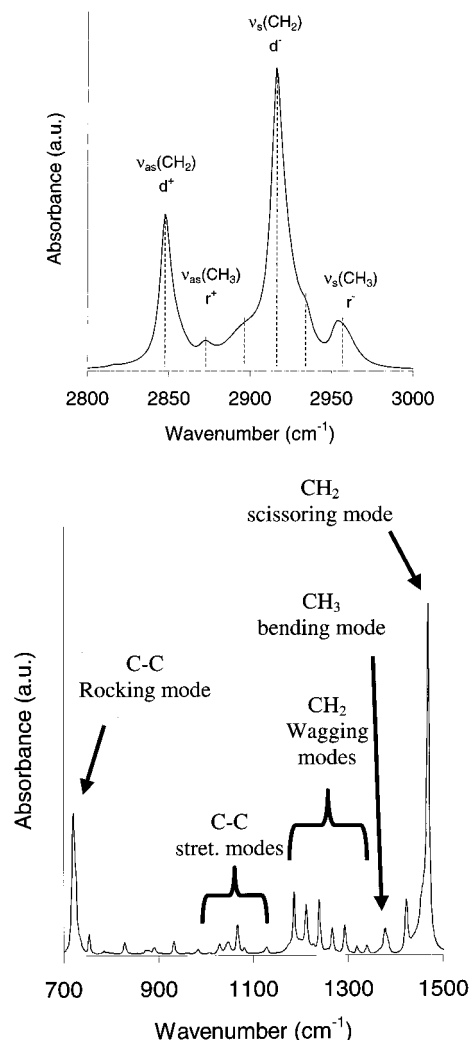


Figure 2. Infrared spectrum of silver dodecanethiolate, $\text{AgS}(\text{CH}_2)_{11}\text{CH}_3$, at 25 °C: (a, top) high-frequency part (2800 – 3000 cm^{-1}) and (b, bottom) low-frequency part (700 – 1500 cm^{-1}).

2918 cm^{-1} for all-trans extended chains^{15,25,28} and in the distinctly different ranges of 2854 – 2856 and 2924 – 2928 cm^{-1} for conformationally disordered chains²⁷ characterized by a significant presence of gauche conformers. On this basis, the observed peak frequencies of 2848 and 2916 cm^{-1} for $\text{AgS}(\text{CH}_2)_{11}\text{CH}_3$ in the room temperature spectrum establish that the alkyl chains are in an all-trans conformational state with little or no significant gauche population. The dominance of all-trans chains in $\text{AgS}(\text{CH}_2)_{11}\text{CH}_3$ is further consistent with the formation of dense, crystalline-like environment for the alkyl chains.²⁸

The lower frequency region (700 – 1500 cm^{-1}) shown in Figure 2b reveals a rich spectral signature composed of a large number of well-defined vibrational mode absorptions. As above, the mode assignments are straightforward. The strongest peak in this region at 1469 cm^{-1} is associated with CH_2 scissoring mode, the one at $\sim 1378\text{ cm}^{-1}$ is assigned to the CH_3 bending or umbrella mode, the well-resolved series of bands in the region 1150 – 1350 cm^{-1} is assigned to the progression series due to CH_2 wagging modes, the less intense, yet distinct progression in the region 1000 – 1150 cm^{-1} is assigned to the skeletal modes of the hydrocarbon chains or C–C–C backbone stretching modes, and lastly the band at 720 cm^{-1} is assigned to the methylene C–H rocking mode. Several attributes of these peaks provide additional diagnosis of the molecular structure of the $\text{AgS}(\text{CH}_2)_{11}\text{CH}_3$ at the room temperature. First, the scissoring

band of the methylene groups ($\delta(\text{CH}_2)$) at $\sim 1469 \text{ cm}^{-1}$ is known to be a sensitive indicator of the alkyl chain packing.^{13,29} It has been previously established that the exact shape of this band including the peak position, width, and the number of components reflects the packing arrangement of the alkyl chain assemblies.³⁰ Specifically, the appearance of a single narrow peak at 1473 or 1467 cm^{-1} is attributed to triclinic or hexagonal subcell packing, respectively. The appearance of well-resolved doublet with two distinct components is known to occur either due to intermolecular vibrational coupling due to a crystal-field splitting in orthorhombic or monoclinic packing or due to the coexistence of triclinic and hexagonal packing in the material. The broad peak in this region is attributed to the inefficient packing of conformationally disorder chains. In the present case, a single narrow band (fwhm $\sim 5.6 \text{ cm}^{-1}$) at 1469 cm^{-1} observed for $\text{AgS}(\text{CH}_2)_{11}\text{CH}_3$ is consistent with the hexagonal subcell packing with a single chain per unit cell in the room temperature structure. Second, in the spectral region between 1150 and 1400 cm^{-1} , the presence of well-resolved progression bands due to CH_2 wagging modes confirms the all-trans structure of the alkyl chains.^{13,31–33} The wag-mode progression series is understood to result from the out-of-phase coupling between the wagging motions of the adjacent methylene units along the chain. This coupling is absent if the chains contain significant gauche conformers and is highly dependent in its number of components, frequencies, and the intensities on the number of correlated methylene oscillators in the chain.

As a function of temperature, all structurally sensitive spectral peaks discussed above undergo pronounced changes in their attributes. These are graphically illustrated in Figure 3, a and b, wherein temperature-dependent infrared spectra of $\text{AgS}(\text{CH}_2)_{11}\text{CH}_3$ for selected temperatures in the range of 25 – $250 \text{ }^\circ\text{C}$ are shown. Specifically, the changes in the precise peak positions, peak widths, and relative intensities provide significant semiquantitative clues regarding the molecular motions associated with the heating of these materials. Quantitative examination of these changes can be correlated with temperature-induced dynamics in the alkyl chain ensembles including mobilities, trans–gauche isomerization, as well as interchain interactions leading to packing reconstructions, such as given below.

The four panels in Figure 4 summarize the thermotropic changes in the peak positions due to methylene symmetric stretching or d^+ at $\sim 2848 \text{ cm}^{-1}$ (Figure 4a), methylene asymmetric stretching or d^- at $\sim 2916 \text{ cm}^{-1}$ (Figure 4b), methylene deformation or scissoring (δ) at $\sim 1467 \text{ cm}^{-1}$ (Figure 4c), and selected, intense modes from the progression series W_k between 1180 and 1320 cm^{-1} (Figure 4d). An examination of these data reveals important aspects of temperature-induced changes in the structure or molecular-level dynamics in the sample system. These are discussed below. The peak position trails of methylene stretches in Figure 4a,b appear correlated and are characterized by six distinct regions. The initial long plateau (I) from 25 to $100 \text{ }^\circ\text{C}$ is essentially horizontal at ~ 2848 and 2916 cm^{-1} in Figure 4, a and b, respectively, reflecting little or no changes in the d^+ and d^- peak positions with temperature in this regime. This, coupled with the low peak position values (see above), indicates that during this warm-up period (25 – $100 \text{ }^\circ\text{C}$), the initial all-trans conformational order of the alkyl chains is preserved. This region is followed by a narrow ramp (II) from 100 to $125 \text{ }^\circ\text{C}$ where the peak positions begin to shift gradually toward higher frequencies reaching ~ 2849 and $\sim 2918 \text{ cm}^{-1}$ at $\sim 125 \text{ }^\circ\text{C}$. These upward shifts in the region II can be assigned to a premelting event characterized by the incipient appearance of gauche conformers. The region

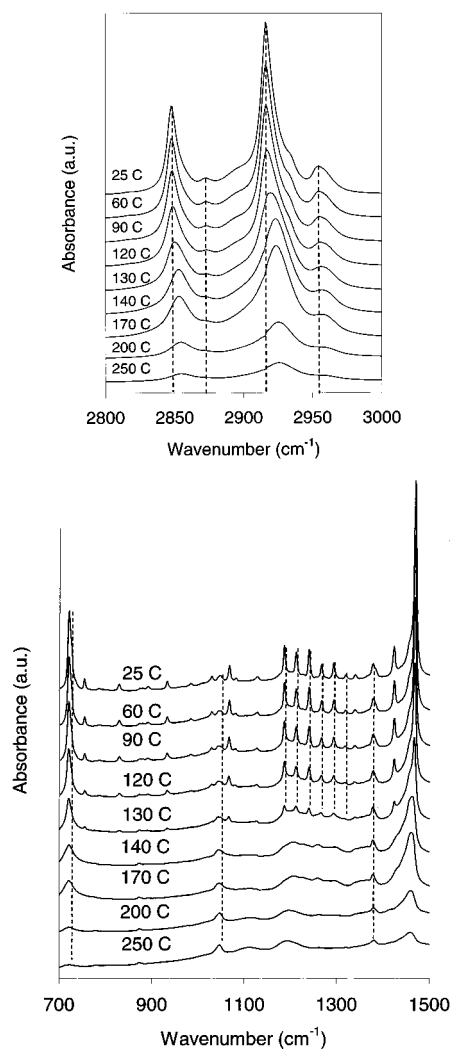


Figure 3. Transmission infrared spectra of silver dodecanethiolate, $\text{AgS}(\text{CH}_2)_{11}\text{CH}_3$, over the temperature range 25 – $250 \text{ }^\circ\text{C}$: (a, top) high-frequency region (2800 – 3000 cm^{-1}) and (b, bottom) low-frequency region (700 – 1500 cm^{-1}).

III of the frequency traces in Figure 4a,b is the most striking one. Here, within a narrow range of temperatures between 125 and $135 \text{ }^\circ\text{C}$, the peak positions jump very abruptly by a large magnitude of 4 – 5 cm^{-1} to assume the values of 2853 and 2923 cm^{-1} at $\sim 135 \text{ }^\circ\text{C}$. This vertical climb signals a rapid accumulation of gauche conformers in the alkyl chain ensembles around $130 \text{ }^\circ\text{C}$, suggesting an abrupt phase transition. Structural implications of this transition will be discussed later in the paper. However, it is important to note here that the values of 2853 and 2923 cm^{-1} above $130 \text{ }^\circ\text{C}$ for the new plateau regions are slightly lower than typically reported for fully disordered chains.²⁷ This region is followed by another plateau (IV) between 135 and $175 \text{ }^\circ\text{C}$ wherein the chain conformational order remains practically unchanged. At $\sim 175 \text{ }^\circ\text{C}$, the peak positions begin to rise again (V), but less abruptly than the region III until the sample temperature of $\sim 200 \text{ }^\circ\text{C}$ is reached. Above $200 \text{ }^\circ\text{C}$, the curve stabilizes at the third plateau (VI) at the highest d^+ and d^- peak position values of ~ 2855 and 2926 cm^{-1} . This second upward shift can be attributed to further disordering of the chains leading to complete conformational disordering of the aliphatic tails comparable to those found for amorphous solids or molecular liquids.³⁴

Analogous shifts near $130 \text{ }^\circ\text{C}$ are also evident for the changes in the scissoring mode frequencies around 1469 cm^{-1} displayed in Figure 4c. Unlike d^+ and d^- peak frequencies, the peak due

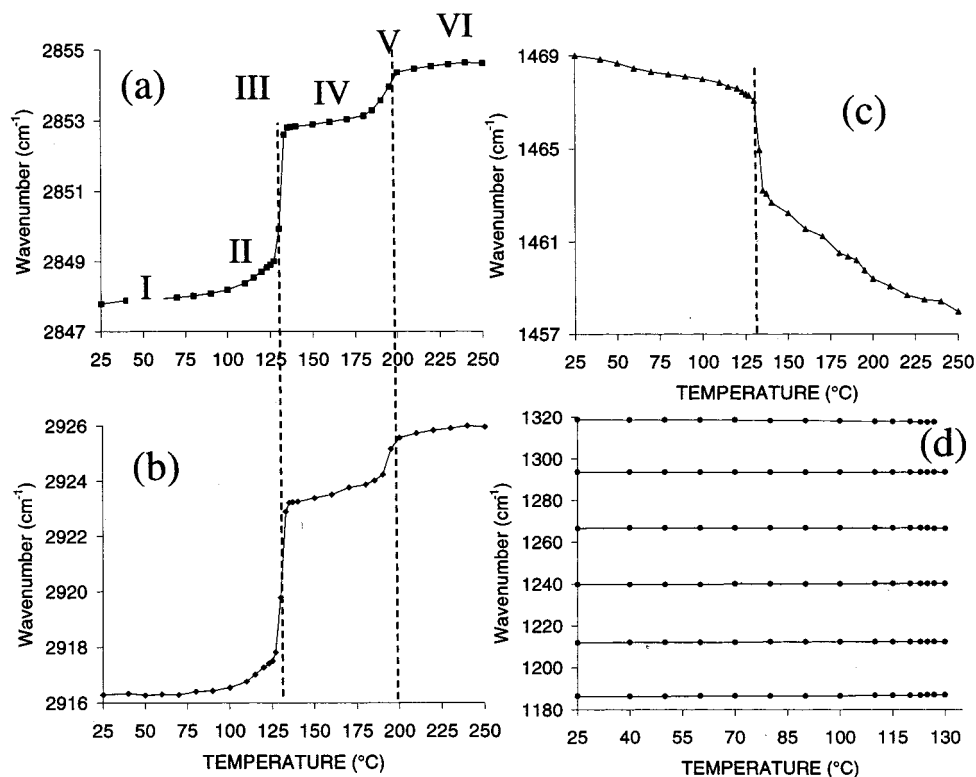


Figure 4. Temperature dependence of the positions of peak maxima due to selected methylene vibrational modes: (a) symmetric C–H stretching mode, (b) asymmetric C–H stretching mode, (c) methylene scissoring mode, and (d) the wagging mode progression series.

to scissoring mode absorption shows a continuous, gradual shift as the temperature is raised with an abrupt drop from ~ 1467 cm^{-1} to 1463 cm^{-1} in the vicinity of the 130 °C where the main structural transition was observed (see above). This drop in frequency, in conjunction with the observed broadening of this peak around the structural transition temperature, can be directly correlated with the disruption of the hexagonal chain packing. Further, note that the secondary irreversible transition, clearly evident in d^+ and d^- trails, is difficult to discern due to the continuous changes in the peak positions in that window of the sample temperature.

For the wagging mode progression series (Figure 4d), the positions of the peak maxima are temperature independent and remain constant to within ± 1 cm^{-1} up to ~ 130 °C. Above this temperature, the peaks could no longer be discerned consistent with the appearance of significant population of gauche conformers (estimated above). The invariance of the W_k peak positions below 130 °C further suggests that no significant accumulation of gauche conformers occurs below the actual structural transition at ~ 130 °C. Previously, it has been shown that the precise separation between the wagging mode peaks in the progression series bears a direct correlation with the number of all-trans conformers in registry. Using a simplified equation,³⁵ $m + 1 = 326/\Delta\nu$, where m is the number of correlated CH_2 units and $\Delta\nu$ the average separation between the W_k peaks, we note that m , estimated at 11.32, in comparison with the actual number of CH_2 units of 11 per chain, further confirms the essentially all-trans structure of the polymethylene chains in AgSR.

The zoomed-in spectrum of $\text{AgS}(\text{CH}_2)_{11}\text{CH}_3$ at 175 °C in the 1300 – 1380 cm^{-1} region shown in Figure 5 illustrates weak but reproducible new features that appear in the intermediate temperature phase (above 130 °C and below 200 °C). For an accurate determination of the peak positions of these bands, we used the second derivative of the absorbance spectra also shown

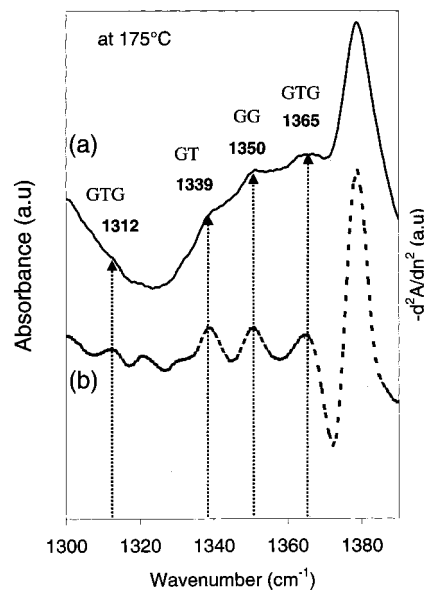


Figure 5. (a) Transmission infrared spectrum of silver dodecanethiolate, $\text{AgS}(\text{CH}_2)_{11}\text{CH}_3$ at 175 °C between 1300 and 1390 cm^{-1} . (b) Second derivative of the infrared spectrum. The arrows point to spectral evidence of conformational gauche defects (G, gauche; GG, double gauche; GTG, kink).

in Figure 5. The traces reveal the presence of peaks at 1339 and 1350 cm^{-1} , and extremely weak features at about 1312 and 1365 cm^{-1} . Corresponding peaks in the high-temperature phases of odd n -alkanes have been previously reported. There, Snyder and co-workers^{36,37} assigned these new peaks to constant-frequency wagging modes due to specific kinds of nonplanar conformers based on the predictions from single-chain calculations. Following these studies, we assign tentatively the observed peaks at 1339 cm^{-1} to end-gauche (GT), the band at 1350 cm^{-1} to double-gauche (GG), and those at 1312 and 1365 cm^{-1} to

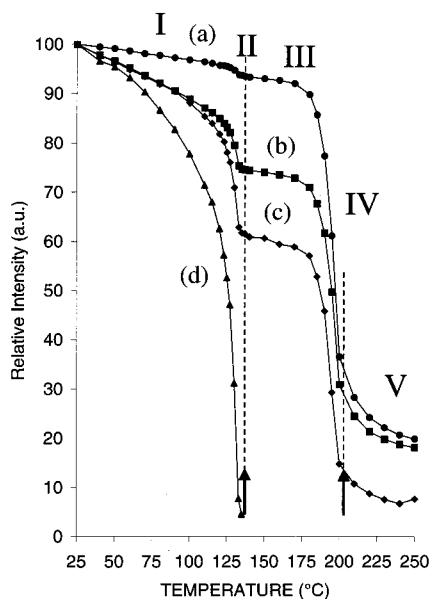


Figure 6. Temperature dependence of the normalized integrated intensity due to selected modes: (a) methylene and methyl C–H stretching modes (2750–3050 cm^{-1}); (b) methylene bending and scissoring modes (1400–1500 cm^{-1}); (c) head band of the rocking mode progression sequence (680–770 cm^{-1}); and (d) head band due to the wagging mode (1180–1196 cm^{-1}) progression series.

kink (GTG) defects, respectively. Because of the weak and ill-resolved nature of these peaks coupled with the ill-defined nature of the background in this region of the spectra, we were unable to quantify the absorbance (and their changes with the sample temperature), precluding any further analysis to estimate the concentration and relative positions of these defects along the polymethylene chain in AgSRs.

The thermotropic behavior of the spectral intensities provides additional information regarding the structural changes. The temperature-dependent evolution of integrated intensity of four distinct regions of the vibrational spectra encompassing selected chain modes is displayed in Figure 6. The integrated intensities were measured by subtracting any background shifts in the spectra, and each peak is independently normalized with respect to its lowest, room temperature intensity values. The four regions chosen include the following: 2800–3000 cm^{-1} region encompassing methylene and methyl C–H stretching modes in Figure 3a; 1400–1500 cm^{-1} region enveloping the methyl and methylene bending and scissoring modes respectively in Figure 3b; 680–770 cm^{-1} region containing the most intense head band of the rocking mode progression near 720 cm^{-1} ; and the 1180–1196 cm^{-1} region containing an arbitrarily chosen wagging mode at $\sim 1188 \text{ cm}^{-1}$. All four traces show a monotonic drop in relative integrated intensities with temperature with the abrupt declines at ~ 130 and ~ 190 °C confirming major structural or phase reconstructions in the vicinity of these temperatures.

The temperature-dependent behavior of the C–H stretching mode intensities in the 2750–3050 cm^{-1} is characterized by five distinct regions as seen in Figure 6a. Even a casual glance of the intensity trace Figure 6a reveals two distinct regions of comparable slopes spanning 25–125 °C (I) and 135–175 °C (III). The two regimes are first separated by a narrow window of temperature (II) (125–135 °C) where a small but rapid decrease in the relative intensity by $\sim 2\%$ is clearly evident. Second, at elevated temperatures (> 175 °C), the second linear region is interrupted by a sudden and rapid decrease in intensity ($\sim 70\%$) up to 210 °C (IV). This region is followed at even higher temperatures by a continuous drop (V), but less dramatic

than in region IV, in spectral intensities. The final intensity at 250 °C is less than 20% of the initial intensity at 25 °C.

The intensity behavior of the methylene and methyl umbrella modes between 1400 and 1500 cm^{-1} is displayed in Figure 6b while that of the rocking mode near 720 cm^{-1} is captured by the trail in Figure 6c which encompasses the frequency range of 680–740 cm^{-1} . These traces are qualitatively comparable to the temperature dependence of C–H stretching modes in Figure 6a and correspondingly show five analogous regions (see previous paragraph). A careful examination of the quantitative differences in these trails yields additional information. First, a comparison of the low-temperature regime (I) reveals that the monotonic drops in intensities of the bending and rocking modes are considerably larger than for C–H stretching modes. This observation supports previous notions that the thermal coefficients of localized oscillators are significantly larger than the delocalized ones.^{38,39} Second, the anomalous intensity losses, for the region II in bending and rocking modes, of 14 and 25%, respectively, are considerably larger than the weak 2% drop observed for methylene stretching modes. Third, note that in the regions III, IV, and IV the slopes or the thermal coefficients for all three modes are quite comparable. Moreover, the actual magnitude of the intensity loss in region IV of ~ 67 and $\sim 83\%$ for bending and rocking modes, respectively, is also quite comparable to 70% estimated for the C–H stretching modes. The final integrated intensities of the bands between 1400–1500 and 680–770 cm^{-1} represent 18% and less than 10% of their initial intensity at the room temperature comparable to 20% seen for the C–H stretching modes.

The intensity behavior of the wagging progression series, illustrated in Figure 6d by the head band between the 1180–1196 cm^{-1} region, displays a gradual and continuous decrease from the normalized room temperature value to $\sim 4.5\%$ at 135 °C where the peak is still observable. Above this temperature, the intensity falls below the noise level in our spectra, and is below our measurable limit ($\sim 1 \times 10^{-5}$ au). A careful examination reveals that the trace is not linear and can be viewed to consist of two regions of distinctly different slopes: the lower temperature region between 25 and 120 °C where the intensity drops to about 60% of its room temperature value and the second 120–135 °C region where the intensity drops from the initial 60% at 120 °C to 4.5% at 135 °C.

Five traces shown in Figure 7 highlight the reversibility characteristics of the temperature-induced changes in long-chain silver thiolates. Traces a, b, and c summarize one thermal cycle involving the heating from room temperature (a) up to 175 °C (b), followed by cooling the sample at the ambient rate which yields the “annealed” spectrum at 25 °C (c). A comparison of the traces in (a) and (c) establishes the essential reversibility of the sample structure during the 25–175 °C thermal cycle. In particular, (1) the return of the conformationally sensitive C–H stretching peak positions, (2) reappearance of the wagging mode progression series, (3) disappearance of the high-temperature defect peaks (see above), (4) the return of the attributes of the packing-sensitive methylene rocking and scissoring modes, and (5) the conservation of the total integrated intensities over the high-frequency range ($[I_c/I_a]_{2800-3000 \text{ cm}^{-1}} \sim 0.98$) as well as the low-frequency range ($[I_c/I_a]_{700-1500 \text{ cm}^{-1}} \sim 1.01$) confirm this conclusion. These slight disparities in the integrated intensities in the C–H stretching region and the low-frequency region, along with concomitant sharpening of methylene C–H stretching peaks and the better resolved nature of the methyl C–H asymmetric peaks,⁴⁰ suggest that the sample annealing leads to

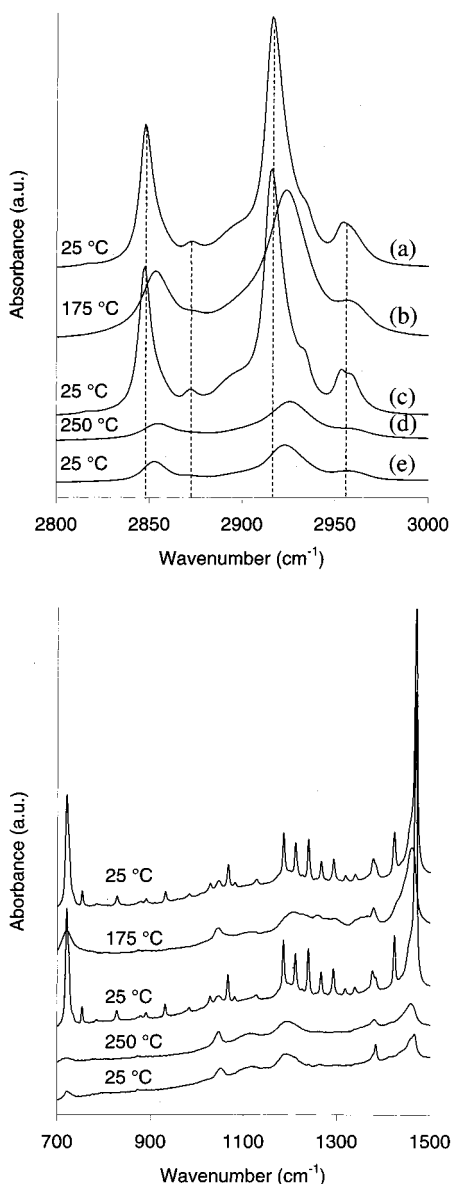


Figure 7. Infrared spectra of silver dodecanethiolate for the highest and the lowest temperatures during two thermal cycles between 25 and 175 °C (a, b, and c traces) and between 25 and 240 °C (c, d, and e traces). Panel A (top) illustrates the high-frequency region (2800–3000 cm^{-1}) and panel B (bottom) shows the spectral changes for the low-frequency region (700–1500 cm^{-1}). The dotted lines are guides to the eye.

small but nonvanishing increase in the ordering and packing of the polymethylene chains. Traces c, d, and e summarize the second thermal cycle involving 25 and 250 °C as end points. The traces clearly reveal that the cycle induced irreversible changes in the sample structure and properties. The spectrum e is qualitatively comparable to the high-temperature spectrum d at 250 °C, proving that upon cooling original intensities could not be regained. This conclusion is best manifest in the integrated intensity ratio over the high- and low-frequency range since the estimated values are ($[I_d/I_a]_{2800-3000 \text{ cm}^{-1}} \sim 0.25$ and $[I_d/I_a]_{700-1500 \text{ cm}^{-1}} \sim 0.50$, then $[I_e/I_d]_{2800-3000 \text{ cm}^{-1}} \sim 0.84$ and $[I_e/I_d]_{700-1500 \text{ cm}^{-1}} \sim 0.92$), respectively. The most plausible explanation for the observed losses in intensities due to the chain modes above is the irreversible degradation of the sample material when heated to 250 °C. This is further confirmed by the irreversible change in the texture of the KBr pellet from initial bright yellow to pale brown upon heating to 250 °C.

Discussion

It is now well appreciated that Fourier transform infrared (FTIR) vibrational spectroscopy is a highly sensitive tool for probing the molecular structure and dynamics of polymethylene chain systems. As mentioned above, a vast body of literature dealing with the IR spectroscopic investigations of simple and substituted *n*-alkanes, alkyl chain based liquid crystals, and long-chain phospholipids provides a firm background with which to decipher accurately the chain-vibrational modes, their inter-relationships with the chain structure, and mobilities in complex polymethylene systems such as the class of long-chain silver *n*-alkanethiolates reported here.

All the evidence presented here can be reconciled in terms of a simple, unified scenario, first postulated by Baena and co-workers²¹ involving mesogenic phase transitions, prompted by the temperature-induced restructuring of the inorganic Ag–S lattice in silver *n*-alkanethiolates. In their study utilizing calorimetric, X-ray, and polarized optical microscopy techniques for a series of long-chain silver *n*-alkanethiolates, Baena and co-workers proposed that at ~ 130 °C the initial bilayer motif is abruptly replaced by a micellar (columnar hexagonal) motif, which at elevated temperatures of ~ 190 °C undergoes a subsequent higher order transition to an amorphous state. The FTIR spectroscopic evidence presented here provides a compelling description of the molecular-level dynamics of polymethylene chain assemblies that attend (as well as precede) these mesogenic transitions, and additionally provides a useful example of the phase behavior of polymethylene assemblies in dimensionally and structurally restrictive media.

Analysis of the room temperature FTIR spectrum (Figure 2) clearly demonstrates that the lamellar structure (bilayer motif) of silver *n*-dodecanethiolate is dominantly populated by all-trans ordered chains at room temperature. This picture of the chain structure is in direct conformity with the previous X-ray diffraction²⁰ and FTIR spectroscopic investigations²³ of AgSRs. As a function of sample temperature, the changes in the FT-IR spectral features of CH_2 stretching, scissoring, wagging, and rocking bands (Figures 3, 4, and 5) provide temperature-induced inter- and intramolecular structural reconstructions on the molecular level.

Bilayer–Micellar Main Phase Transition. At the previously assigned temperature of ~ 130 °C for the bilayer–micellar phase transition, all conformationally sensitive characteristic chain modes signal rapid and abrupt changes in the structures of the sandwiched chain assemblies. In particular, the phase transition is attended by drastic shifts in methylene stretching mode peak frequency positions, considerable broadenings of these peaks, and the disappearance of the wagging progression bands (Figure 4). Taken together, these changes establish that the alkyl chains in the AgSR ensembles establish that the bilayer–micellar phase transition is accompanied by a rapid intramolecular trans–gauche isomerization event leading to a significant population of gauche conformers in the bimolecular chain assemblies above the transition temperature. It is in order here to recall that the occurrence and general location of gauche defects along the chain can be monitored by the appearance of new wagging mode peaks due to isolated gauche defects in the 1300–1360 cm^{-1} range. Indeed, a careful examination of the spectra above 130 °C (Figure 3b) reveals the appearance of new bands near 1339, 1350, and 1312, and 1365 cm^{-1} . The latter bands, in conjunction with the previous studies of defect bands in *n*-alkanes,^{26,36,37} can be assigned to end-gauche (GT) (taking place probably at the end of chains), double-gauche (GG), and kink (GTG) defects, respectively.

It is additionally instructive to note that all the peak changes are further consistent with the formation of partially disordered (rather than fully collapsed) alkyl chain structure above 130 °C. For example, the peak positions of methylene stretching modes assume the values of 2853 and 2923 cm^{-1} intermediate to those observed for crystalline *n*-alkanes^{15,25,28} (2846–2850 and 2915–2918 cm^{-1}) and liquid *n*-alkanes²⁷ (2854–2856 and 2924–2928 cm^{-1}). Similarly, the nonvanishing contribution from the methylene scissoring mode at $\sim 1465 \text{ cm}^{-1}$ is further consistent with only partially disordered chain structure. Moreover, the solid–solid bilayer–micellar phase transition is also characterized by a rapid change in the packing-sensitive methylene scissoring mode positions (Figure 4c) as well as anomalous declines in intensities of the conformationally sensitive modes (Figure 6). These changes have been previously observed in the studies of *n*-alkane^{26,37,38,41} and related systems^{16,42} and are typically ascribed to the changes in the intermolecular packing of the polymethylene chains at the order–disorder transition.⁴³ Finally, the observed transition was noted to be fully reversible (Figure 7) in multiple thermal cycles confirming the equilibrium thermodynamic nature of this transition.

Micellar–Amorphous Transition. The higher order transition at $\sim 190 \text{ }^\circ\text{C}$, assigned to the micellar–amorphous phase transition from earlier²¹ calorimetric, X-ray diffraction, and optical microscopy measurements, is also attended by the changes in the chain structure and ordering. Peak position changes in the methylene stretches (Figure 4a,b) unambiguously reveal that this transition is characterized by significant changes in the gauche population in the polymethylene ensembles. Specifically, the transition renders the methylene stretching peak positions to assume the values of 2855 and 2926 cm^{-1} , values typically assigned to liquidlike collapse of alkyl chain or amorphous unstructured packing. However, the dramatic irreversible changes (Figure 7) about this secondary transition in all chain modes indicate that the transition is not an equilibrium thermodynamic event, but is most likely due to thermal degradation of the material (e.g., decarboxylation and oxidation of the hydrocarbon chains). Such degradation could provide sufficient additional free volume to understand the observed frequency shifts in methylene stretches and radical loss of intensity up to $\sim 70\%$.

Pretransitional Chain Dynamics. A subtle, but unmistakable premelting event is seen in the *T*-dependent C–H stretching trails shown in Figure 4 as well as in the intensity variations shown in Figure 6. Region II in the methylene stretches between 100 and 125 °C forewarns the incipient bilayer–micellar transition at 133 °C. In this narrow temperature window, rather rapid accumulation of gauche conformers is evident. However, the wagging mode progression series which diminishes in intensity gradually over the entire pretransitional *T* range, 25–130 °C (Figure 6), at first appears contradictory, but the correlations between wagging mode intensities and the emergence of gauche conformers in polymethylene chains are known to be highly nonlinear and dependent on the precise location of the gauche sequences. For example, a small amount of gauche disorder in the chain interior can cause the wagging mode intensities to completely vanish.⁴⁴ In this regard, the observed gradual diminution of the wagging mode intensities in the pretransitional window may not contradict the inference we derive from the frequency trails of the methylene C–H stretches in the pretransitional regime. Note that the existence of pretransitional window predicted from Figures 4ab and 5 appears comparable to premelting phenomena observed previously in chain assemblies of odd alkanes.^{26,32,41}

Effects of the Proximal Organic–Inorganic Interface. The pinning of the aliphatic chains to the rigid Ag–S backbone in silver dodecanethiolates introduces many peculiarities in its phase behavior. First, the silver alkanethiolates undergo only solid–solid transitions and actual melting to a liquid state does not seem to occur before thermal degradation. This is in sharp contrast to the typical phase behavior of comparable *n*-alkanes which show distinct solid–liquid transitions within the temperature range studied. Second, in comparison with analogous *n*-alkanes,^{26,38} and layered compounds,^{3b,30b} we note that the chain dynamics in silver thiolates is severely restricted. The melting of alkyl chain assemblies in the former compounds is generally known to be preceded by a combination of lateral (intralamellar) and transverse (interlamellar) mobilities of the chains. These mobilities are significantly restricted in silver alkanethiolates due to strong covalent pinning to the Ag–S network causing considerably reduced span of pretransitional chain dynamics (e.g., considerably lower isolated defect contents in chains before the main transitions) and an apparent absence of the interlamellar dynamics⁴⁵ evident in our study. Finally, we note that the only prominent reversible transition, attributed previously to a bilayer micellar motif conversion, is guided by the mesoscopic reconstruction of the inorganic Ag–S backbone from its initial trigonal to linear coordination (μ^3 to μ^2) and the ensuing chain dynamics appears only to conform to this reconstruction rather than direct the phase behavior. Such a picture is strongly supported by the previous observation by Baena and co-workers²¹ that the exact value of this main transition is quasi-independent of the chain length in a fairly large range from hexyl to octadecyl chains.⁴⁶

Conclusions

Using temperature-dependent Fourier transform infrared spectroscopy, we examined the dynamics of aliphatic chains in layered inorganic–organic silver dodecanethiolate, $\text{AgS}(\text{CH}_2)_{11}\text{CH}_3$, in repeated thermal cycling between 25 and 250 °C. Results presented here confirm that the sandwiched bimolecular chain assemblies in $\text{AgS}(\text{CH}_2)_{11}\text{CH}_3$ are predominantly in all-trans conformations at room temperature. The central result of this study is the observation of an abrupt, but fully reversible conformational transition at $\sim 130 \text{ }^\circ\text{C}$. This is caused by a rapid rise in the gauche conformers between 125 and 135 °C with a concomitant change in the packing of the aliphatic tails from an initial, efficient hexagonal type to the final one characterized by a highly disordered packing of partially aligned alkyl chains. These observations are consistent with the earlier predictions of the abrupt mesoscopic change in the structural motif from bilayer to micellar geometry at $\sim 130 \text{ }^\circ\text{C}$. Further, present data reveal a weak, but distinct “premelting” window between 100 and 125 °C wherein the gradual accumulation of gauche conformers appears to prepare the material system for the incipient phase transition at 130 °C. Upon further heating above 200 °C, the aliphatic chains in the silver dodecanethiolate irreversibly disorders into an amorphous or a liquidlike state with highly disordered alkyl chains. The irreversibility of the latter transition signals that this second transition at 190 °C is associated with the thermal degradation of the material. The conformational dynamics during the thermal melting of silver dodecanethiolates elucidated here clearly portray the role of the organic–inorganic interface in these fully covalently bonded network structures: unlike simple and substituted *n*-alkanes, silver alkanethiolates only undergo an order–order phase transition at significantly elevated temperatures ($\sim 130 \text{ }^\circ\text{C}$) that is chain length invariant and can be associated with the

mesoscale buckling (or collapse) of the inorganic framework (Ag–S) rather than the relative motion of individual chains within the crystal.

Acknowledgment. This research was supported by the LDRD program at Los Alamos National Laboratory.

References and Notes

- (1) For example, see: (a) International School of Physics “Enrico Fermi” (1983: Varenna, Italy). In *Physics of amphiphiles—micelles, vesicles, and microemulsions*; Degiorgio, V., Corti, M., Eds.; Elsevier Science Pub. Co.: New York, 1985. (b) Yada, M.; Hiyoshi, H.; Ohe, K.; Machida, M.; Kijima, T. *Inorg. Chem.* **1997**, *36*, 5565. (c) Machida, M.; Kijima, T. *Inorg. Chem.* **1998**, *37*, 6470.
- (2) (a) Kazei, Z. A.; Krynetskii, I. B. In *Magnetic properties of nonmetallic inorganic compounds based on transition elements. Perovskite-type layered cuprates (high-*T_c* superconductors and related compounds)*; Wijn, H. P. J., Ed.; Springer-Verlag: New York, 1994. (b) Braun, M.; Tuffentsammer, W.; Wachtel, H.; Wolf, H. C. *Chem. Phys. Lett.* **1999**, *303*, 157. (c) Era, M.; Maeda, K.; Tsutsui, T. *Thin Solid Films* **1998**, *331*, 285. (d) Era, M.; Maeda, K.; Tsutsui, T. *Chem. Phys. Lett.* **1998**, *296*, 417.
- (3) (a) Whittingham, M. S.; Jacobson, A. J. In *Intercalation chemistry*; Whittingham, M. S., Jacobson, A. J., Eds.; Academic Press: New York, 1982. (b) Basini, L.; Raffaelli, A.; Zerbi, G. *Chem. Mater.* **1990**, *2*, 679. (c) Giannelis, E. P. *Adv. Mater.* **1996**, *8*, 29. (d) Alberti, G.; Casciola, M.; Costantino, U.; Viviani, R. *Adv. Mater.* **1996**, *8*, 291. (e) Choy, J. H.; Kwon, S. J.; Park, G. S. *Science* **1998**, *280*, 1589.
- (4) (a) Roberts, G. G. In *Langmuir–Blodgett films*; Roberts, G., Ed.; Plenum Press: New York, 1990. (b) Rabe, J. P.; Swalen, J. D.; Rabolt, J. F. *J. Chem. Phys.* **1987**, *86*, 1601. (c) Tippmann-Krayer, P.; Kenn, R. M.; Mohwald, H. *Thin Solid Films* **1992**, *210/211*, 577.
- (5) (a) de Gennes, P. G.; Prost, J. In *The physics of liquid crystals*; de Gennes, P. G., Prost, J., Eds.; Oxford University Press: New York, 1993. (b) Kajiyama, T. *J. Macromol. Sci.-Chem.* **1988**, *A25*, 583. (c) Chou, C. F.; Jin, A. J.; Hui, S. W.; Huang, C. C.; Ho, J. T. *Science* **1998**, *280*, 1424.
- (6) (a) Fendler, J. H. In *Membrane-mimetic approach to advanced materials*; Fendler, J. H., Ed.; Springer-Verlag: New York, 1994. (b) Plant, A. L.; Brigham-Burke, M.; Petrella, E. C.; O’Shannessy, D. J. *Anal. Biochem.* **1995**, *226*, 342. (c) Bunjes, N.; Schmidt, E. K.; Jonczyk, A.; Rippmann, F.; Beyer, D.; Ringsdorf, H.; Gräber, P.; Knoll, W.; Naumann, R. *Langmuir* **1997**, *13*, 6188.
- (7) (a) Ulman, A. In *An introduction to ultrathin organic films: from Langmuir–Blodgett to self-assembly*; Ulman, A., Ed.; Academic Press: Boston, 1991. (b) Laibinis, P. E.; Whitesides, G. M.; Allara, D. L.; Tao, Y. T.; Parikh, A. N.; Nuzzo, R. G. *J. Am. Chem. Soc.* **1991**, *113*, 7152. (c) Thompson, W. R.; Cai, M.; Ho, M.; Pemberton, J. E. *Langmuir* **1997**, *13*, 2291. (d) Yam, C. M.; Tong, S. S. Y.; Kakkar, A. K. *Langmuir* **1998**, *14*, 6941. (e) Thome, J.; Himmelhaus, M.; Zharnikov, M.; Grunze, M. *Langmuir* **1998**, *14*, 7435. (f) Schoenfish, M. H.; Pemberton, J. E. *J. Am. Chem. Soc.* **1998**, *120*, 4502.
- (8) Smith, E. L.; Porter, M. D. *J. Phys. Chem.* **1993**, *97*, 8032.
- (9) Aksay, I. A.; Trau, M.; Manne, S.; Honma, I.; Yao, N.; Zhou, L.; Fenter, P.; Eisenberger, P. M.; Gruner, S. M. *Science* **1996**, *273*, 892.
- (10) (a) Cao, G.; Hong, H.-G.; Mallouk, T. E. *Acc. Chem. Res.* **1992**, *25*, 420. (b) Lacroix, P. G.; Clement, R.; Nakatani, Keitaro; Zyss, J.; Ledoux, I. *Science* **1994**, *263*, 658.
- (11) (a) Vermeulen, L. A.; Thompson, M. E. *Nature* **1992**, *358*, 656. (b) Vermeulen, L. A. *Prog. Inorg. Chem.* **1997**, *44*, 143.
- (12) (a) Laget, V.; Hornick, C.; Rabu, P.; Drillon, M.; Ziessel, R. N. *Coord. Chem. Rev.* **1998**, *180*, 1533. (b) Laget, V.; Hornick, C.; Rabu, P.; Drillon, M.; Turek, P.; Ziessel, R. N. *Adv. Mater.* **1998**, *10*, 1024.
- (13) Snyder, R. G. In *Methods of Experimental Physics*; Marton, L., Marton, C., Eds.; Academic: New York, 1980.
- (14) (a) Mantsch, H. H.; Martin, A.; Cameron, D. G. *Biochemistry* **1981**, *20*, 3138. (b) Maroncelli, M.; Strauss, H. L.; Snyder, R. G. *J. Chem. Phys.* **1985**, *82*, 2811.
- (15) Snyder, R. G.; Schachtschneider, J. H. *Spectrochim. Acta* **1963**, *19*, 85.
- (16) Cameron, D. G.; Casal, H. L.; Mantsch, H. H. *Biochemistry* **1980**, *19*, 3665.
- (17) Mendelsohn, R.; Davies, M. A.; Brauner, J. W.; Schuster, H. F.; Dluhy, R. A. *Biochemistry* **1989**, *28*, 8934.
- (18) (a) Halperin, B. I.; Nelson, D. R. *Phys. Rev. Lett.* **1978**, *41*, 121. (b) Nelson, D. R.; Halperin, B. I. *Phys. Rev.* **1979**, *B19*, 2456.
- (19) Evolution of translational order parameter in such tethered systems requires the breaking of strong, network covalent bonds.
- (20) Dance, I. G.; Fisher, K. J.; Herath Banda, R. M.; Scudder, M. L. *J. Am. Chem. Soc.* **1991**, *30*, 183.
- (21) Baena, M. J.; Espinet, P.; Lequerica, M. C.; Levelut, A. M. *J. Am. Chem. Soc.* **1992**, *114*, 4182.
- (22) Fijolek, H. G.; Grohal, J. R.; Sample, J. L.; Natan, M. J. *Inorg. Chem.* **1997**, *36*, 622. (b) Fijolek, H. G.; Gonzalez-Duarte, P.; Park, S. H.; Sui, S. L.; Natan, M. J. *Inorg. Chem.* **1997**, *36*, 5299.
- (23) Parikh, A. N.; Gillmor, S. D.; Beers, J. D.; Beardmore, K. M.; Cutts, R. W.; Swanson, B. I. *J. Phys. Chem.* **1999**, *B103*, 2850.
- (24) Hudson, S. A.; Maitlis, P. M. *Chem. Rev.* **1993**, *93*, 861.
- (25) Snyder, R. G.; Hsu, S. L.; Krimm, S. *Spectrochim. Acta* **1978**, *34*, 395.
- (26) Zerbi, G.; Magni, R.; Gussoni, M.; Moritz, K. H.; Bigotto, A.; Dirlikov, S. *J. Chem. Phys.* **1981**, *75*, 3175.
- (27) Snyder, R. G.; Strauss, H. L.; Elliger, C. A. *J. Phys. Chem.* **1982**, *86*, 5145.
- (28) Macphail, R. A.; Strauss, H. L.; Snyder, R. G.; Elliger, C. A. *J. Phys. Chem.* **1984**, *88*, 334.
- (29) Hagemann, H.; Snyder, R. G.; Peacock, A. J.; Mandelkern, L. *Macromolecules* **1989**, *22*, 3600.
- (30) (a) Borja, M.; Dutta, P. K. *J. Phys. Chem.* **1992**, *96*, 5434; Snyder, R. G. *J. Mol. Spectrosc.* **1961**, *7*, 116. (b) Almirante, C.; Minoni, G.; Zerbi, G. *J. Phys. Chem.* **1986**, *90*, 852.
- (31) Snyder, R. G. *J. Mol. Spectrosc.* **1960**, *4*, 411.
- (32) Senak, L.; Moore, D.; Mendelsohn, R. *J. Phys. Chem.* **1992**, *96*, 2749.
- (33) Naselli, C.; Rabe, J. P.; Rabolt, J. F.; Swalen, J. D. *Thin Solid Films* **1985**, *134*, 173.
- (34) Dorset, D. L.; Strauss, H. L.; Snyder, R. G. *J. Phys. Chem.* **1991**, *95*, 938.
- (35) Parikh, A. N.; Liedberg, B.; Atre, S. V.; Ho, M.; Allara, D. L. *J. Phys. Chem.* **1995**, *99*, 9996.
- (36) (a) Snyder, R. G. *J. Chem. Phys.* **1967**, *47*, 1316. (b) Snyder, R. G.; Maroncelli, M.; Qi, S. P.; Strauss, H. L. *Science* **1981**, *214*, 188.
- (37) (a) Maroncelli, M.; Qi, S. P.; Strauss, H. L.; Snyder, R. G. *J. Am. Chem. Soc.* **1982**, *104*, 6237. (b) Hagemann, H.; Strauss, H. L.; Snyder, R. G. *Macromolecules* **1987**, *20*, 2810.
- (38) Casal, H. L.; Mantsch, H. H.; Cameron, D. G. *J. Chem. Phys.* **1982**, *77*, 2825.
- (39) Snyder, R. G.; Maroncelli, M.; Strauss, H. L.; Hallmark, V. M. *J. Phys. Chem.* **1986**, *90*, 5623.
- (40) Note the splitting of the modes in the annealed spectrum at 25 °C (c). This splitting has been previously attributed to hindered rotation of CH₃ groups in the motionally narrowed limit: (a) Snyder, R. G.; Macphail, R. A.; Strauss, H. L. *Bull. Am. Phys. Soc.* **1981**, *26*, 360. (b) Macphail, R. A.; Snyder, R. G.; Strauss, H. L. *J. Chem. Phys.* **1982**, *77*, 1118.
- (41) Casal, H. L.; Cameron, D. G.; Mantsch, H. H. *Can. J. Chem.* **1983**, *61*, 1736.
- (42) Hollenberg, J. L.; Dows, D. A. *J. Chem. Phys.* **1962**, *37*, 1300.
- (43) (a) Abbate, S.; Gussoni, M.; Zerbi, G. *J. Chem. Phys.* **1979**, *70*, 3577; (b) Gussoni, M.; Abbate, S.; Dragoni, B.; Zerbi, G. *J. Mol. Struct.* **1980**, *61*, 355.
- (44) Senak, L.; Moore, D.; Mendelsohn, R. *J. Phys. Chem.* **1992**, *96*, 2749–2754.
- (45) At room temperature, the system can be described to consist of periodic lamellar structure with planes of Ag–S separated by a dense assembly of hydrocarbon chains in an all-trans conformation. As the temperature is raised, the interlamellar forces decrease. The band at 1378 cm⁻¹, which is assigned to the CH₃ bending mode, is sensitive to the interlamellar interactions (ref 26). Over the temperature range 25–190 °C, the peak maxima of this mode (not shown here) increase only slightly (~1 cm⁻¹). By comparison, *n*-nonadecane²⁶ reveals a shift of approximately 3.5 cm⁻¹ from the value of 1375–1378.5 cm⁻¹ at the main phase transition which occurs at about 23 °C. The close correspondence between the room temperature value of 1378 cm⁻¹ for silver dodecanethiolate and the post-transition value of 1378.5 cm⁻¹ in nonadecane may hint that the interlamellar interactions in silver dodecanethiolates are already weakened at the room temperature.
- (46) Our recent FTIR measurements confirm the chain-length independence of the temperature of this main solid–solid (bilayer–micellar) transition (Bardeau, J.-F.; Parikh, A. N.; Beers, J. D.; Swanson, B. I. Unpublished material, 1999).